Impact of Realistic Bus Frequency Measurements on Wide-Area Power System Stabilizers

Georgios Tzounas, Muyang Liu, Mohammed Ahsan Adib Murad, Federico Milano
School of Electrical and Electronic Engineering,
University College Dublin, Ireland
{georgios.tzounas, muyang.liu, mohammed.murad}@ucdconnect.ie, federico.milano@ucd.ie

Abstract—The paper studies the dynamic response of a Wide-Area Power System Stabilizer (WAPSS) for damping inter-area oscillations. The WAPSS utilizes remote bus frequency measurements obtained with frequency estimations. The geometric approach is adopted for the selection of the most effective signal and input placement. Then, the suitability of Padé approximants to capture the impact of communication delays on signals observability is tackled. The results of the small-signal stability analysis are discussed through non-linear time domain simulations with inclusion of time-varying stochastic delays.

Index Terms—Inter-area oscillations, wide-area signals, frequency estimation, observability/controllability, time delays, transient stability analysis.

I. INTRODUCTION

A. Motivation

Feedback signal and input location selection are critical decisions during a control design and often not straightforward to be made, especially when communication networks mediate between measurements and control. A relevant example of this kind are Power System Stabilizers (PSSs) coupled with Wide-Area Measurement Systems (WAMS). The utilization of available signals from the transmission system as well as the study of communication delays impact on control signal selection have motivated this work.

B. Literature Review

Low frequency oscillations are inherent in interconnected power systems and are caused by poorly damped modes. Power systems show both local modes with a single or a group of generators oscillating within an area (typically 1-2 Hz) and inter-area modes with a group of generators oscillating with respect to a group of a different area (typically 0.1-1 Hz) [1].

The standard solution for suppressing the local oscillation modes is the installation of PSSs with local signals [1]. On the other hand, effective damping of inter-area modes usually requires the inclusion of remote signals [2]. This is because inter-area modes are often observable from a local signal but effectively controllable only from another location [3]. With the development of WAMS and the broad deployment of Phasor Measurement Units (PMUs), remote signals can be

obtained and transmitted to a Wide-Area Damping Controller (WADC) through a communication network [4].

The evaluation of wide-area signals plays an important role in the design of a WADC. The comparison of two common modal observability/controllability methods, namely the residues and the geometric approach, has deduced that the signals recommended by the geometric approach can always obtain the best robustness and performance [5]. Thus, the geometric approach is adopted in the present work. Concerning frequency-based WADCs, the results in [2], [6], [7] show that inter-area oscillations are better observable through the differential rotor speed of two machines from different areas. However, PMUs are installed on system buses and, typically, only bus frequency measurements are available to a WADC. In this paper, we consider both ideal and Phase-Locked Loop (PLL) estimated bus frequency measurements.

The involvement of the communication network in remote signal transmission introduces time delays with inclusion of noise, data disordering and dropout [8], [9]. Despite the fact that eigen-based methods have been succesfully applied to approximate the spectrum of power systems modeled with Delay Differential Algebraic Equations (DDAE) [10], [11], global modal analysis of delayed power systems is still an open research topic. An approximation of the effect of delays on the observability of wide-area signals can be provided using Padé polynomials [12]. We evaluate the accuracy of such an approach with a detailed delay model that is able to emulate the physical behavior of WAMS [13].

C. Contributions

The contributions of the paper are twofold.

- A comparison of the dynamic behavior of WAPSSs using either ideal bus frequency signals or PLL-based estimations. Ideal signals are obtained with the frequency divider proposed in [14]. Estimations are obtained with the commonly used Synchronous Reference Frame PLL (SRF-PLL) [15].
- A discussion on the suitability of Padé approximants to capture the effect of delays on wide-area signals observability. Conclusions are drawn based on non-linear time domain simulations with inclusion of realistic WAMS delays [13].

D. Organization

The remainder of the paper is organized as follows. Section II recalls the state space model of power systems and presents the applied control scheme. Section III outlines the delay models utilized in this work. Section IV discusses the case study by carrying modal and transient stability analyses on the two-area test system. Conclusions are drawn in Section V.

II. POWER SYSTEM MODEL AND CONTROL SCHEME

A. State Space Representation

Power systems are conventionally described through a set of Differential Algebraic Equations (DAEs):

$$\dot{x} = f(x, y, u)$$
$$0 = g(x, y, u) , \qquad (1)$$

where f ($f : \mathbb{R}^{n+m+p} \to R^n$), g ($g : \mathbb{R}^{n+m+p} \to R^m$) are the differential and algebraic equations; x, $x \in \mathbb{R}^n$, and y, $y \in \mathbb{R}^m$, are the state and algebraic variables, respectively; and u, $u \in \mathbb{R}^p$, are the controlled inputs.

Differentiating (1) around an equilibrium point (x_0, y_0, u_0) yields:

$$\Delta \dot{x} = f_x \Delta x + f_y \Delta y + f_u \Delta u$$
$$0 = g_x \Delta x + g_y \Delta y + g_u \Delta u , \qquad (2)$$

where f_x, f_y, f_u, g_x, g_y and g_u are the system Jacobian matrices; $\Delta x = x - x_0$, $\Delta y = y - y_0$ and $\Delta u = u - u_0$. The Multiple-Input Multiple-Output (MIMO) state space representation of the system is:

$$\Delta \dot{x} = A \Delta x + B \Delta u$$
$$\Delta w = C \Delta x + D \Delta u , \qquad (3)$$

where $A = f_x - f_y g_y^{-1} g_x$, $B = f_u - f_y g_y^{-1} g_u$ and w are output measurements.

B. Modal Analysis

The modes of the open-loop power system $\Delta \dot{x} = A \Delta x$ can be obtained by solving the characteristic equation $\det(A - \lambda I) = 0$. The corresponding right and left eigenvectors associated with a mode λ_k are determined by solving $A \phi_k = \lambda_k \phi_k$ and $\psi_k A = \lambda_k \psi_k$, respectively. That said, the geometric observability/controlability are defined as follows [16].

The geometric observability $gm_{o\mu}(k)$ of the mode λ_k from output w_μ is:

$$gm_{o\mu}(k) = \cos(\theta_1(c_\mu^T, \phi_k)) = \frac{|c_\mu \phi_k|}{||\phi_k|| \, ||c_\mu||} , \qquad (4)$$

where c_μ is the μ_{th} row of the output matrix C; θ_1 is the acute angle between c_μ and the right eigenvector ϕ_k; $|\cdot|$ and $||\cdot||$ are the modulus and Euclidian norm, respectively.

The geometric controllability $gm_{c\nu}(k)$ of the mode λ_k from input u_ν is:

$$gm_{c\nu}(k) = \cos(\theta_2(\psi_k, b_\nu)) = \frac{|b_\nu \psi_k|}{||\psi_k|| \, ||b_\nu||} , \qquad (5)$$

where b_ν is the ν_{th} column of the input matrix B; θ_2 is the acute angle between b_ν and the left eigenvector ψ_k.

Based on these measures, a comparison among different outputs and inputs can be carried out, so that the ones that provide the maximum joint geometric observability/controllability measure are selected. The joint observability/controllability measure is defined by:

$$gm_{cok}(\mu, \nu) = gm_{c\nu}(k) \, gm_{o\mu}(k) . \qquad (6)$$

C. Wide-Area Power System Stabilizer (WAPSS) Model

The WAPSS in this study is a decentralized controller installed at the j_{th} synchronous machine. The wide-area stabilizing signal v_{si} is a differential frequency of the form:

$$v_{si} = \omega_{\text{B}i} - \omega_{\text{G}j} , \qquad (7)$$

where $\omega_{\text{G}j}$ is the local rotor speed of the j_{th} synchronous machine; $\omega_{\text{B}i}$ is the frequency at bus i.
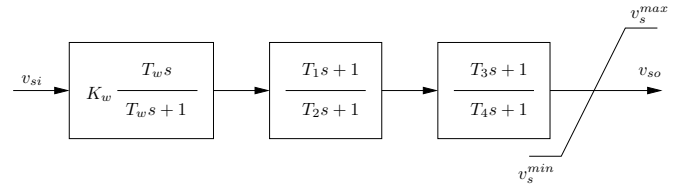

Fig. 1: WAPSS block diagram.

The structure of the WAPSS (see Fig. 1) can be described by the following set of DAEs:

$$\dot{v}_1 = -(K_w v_{si} + v_1)/T_w$$
$$\dot{v}_2 = ((1 - \frac{T_1}{T_2})(K_w v_{si} + v_1) - v_2)/T_2$$
$$\dot{v}_3 = ((1 - \frac{T_3}{T_4})(v_2 + \frac{T_1}{T_2}(K_w v_{si} + v_1)) - v_3)/T_4 \qquad (8)$$
$$0 = v_3 + \frac{T_3}{T_4}(v_2 + \frac{T_1}{T_2}(K_w v_{si} + v_1)) - v_{so} ,$$

where K_w is the WAPSS gain, T_w is the washout time constant, T_1, T_2, T_3, T_4 are the 4 stabilizing blocks time constants, v_1, v_2, v_3 are the WAPSS state variables and v_{so} the output signal. The output signal v_{so} is an additional input to the local Automatic Voltage Regulator (AVR) initial reference (v_0^{ref}), so that the controller damps electromechanical oscillations through excitation control. The resulting voltage reference (v^{ref}) is:

$$v^{\text{ref}} = v_0^{\text{ref}} + v_{so} . \qquad (9)$$

D. Bus Frequency Estimation

In order to obtain the wide-area signal in (7), an estimation of the frequency $\omega_{\text{B}i}$ is required. To this aim, we utilize the commonly used SRF-PLL (see Fig. 2) model. In Fig. 2, the constant delay implies that the bus phase angle ($\theta_{\text{B}i}$) measurement is not instantaneous. The error between the measured and estimated phase angle is fed to a Proportional-Integral (PI) controller, which outputs the estimated bus frequency deviation ($\Delta \tilde{\omega}_{\text{B}i}$). The frequency at bus i is obtained as:

$$\tilde{\omega}_{\text{B}i} = \omega_0 + \Delta \tilde{\omega}_{\text{B}i} , \qquad (10)$$
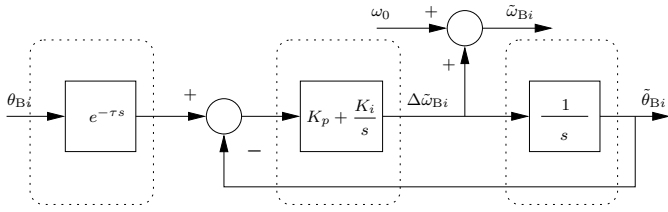
Fig. 2: SRF-PLL block diagram.

where ω_0 is the fundamental frequency of the system.

PLL-based frequencies are accurate but include a compromise between noise and speed of response. They are also prone to problems during the numerical integration [15].

In this work, we compare the results obtained with the SRF-PLL with the ones produced when ideal bus frequency estimations are used. Ideal bus frequencies are estimated using the frequency divider formula (FDF) proposed in [14]. FDF is a general expression which allows the estimation of the frequency at the buses of a transmission system. In per units, the FDF is formulated as:

$$\boldsymbol{\omega}_{\mathrm{B}} = \mathbf{1} - (\boldsymbol{B}_{\mathrm{BB}} + \boldsymbol{B}_{\mathrm{B0}})^{-1}\boldsymbol{B}_{\mathrm{BG}}(\boldsymbol{\omega}_{\mathrm{G}} - \mathbf{1}) \ , \qquad (11)$$

where $\boldsymbol{\omega}_{\mathrm{B}}$ are the estimated bus frequencies; $\boldsymbol{\omega}_{\mathrm{G}}$ are the synchronous machines rotor speeds; $\boldsymbol{B}_{\mathrm{BB}}$, $\boldsymbol{B}_{\mathrm{B0}}$, $\boldsymbol{B}_{\mathrm{BG}}$ are system susceptance matrices. The accuracy, the numerical robustness and the computational efficiency of the FDF have been discussed in [14], [17] and [18].

III. TIME DELAY MODELS

A. DDAEs and WAMS delays

Introducing time delays in (1) changes the set of DAEs into a set of DDAEs. For the purpose of this paper, the index-1 Hessenberg is an adequate formulation to model power systems with delays [19]:

$$\begin{aligned} \dot{\hat{\boldsymbol{x}}} &= \hat{\boldsymbol{f}}(\hat{\boldsymbol{x}}, \hat{\boldsymbol{y}}, \hat{\boldsymbol{x}}_d, \hat{\boldsymbol{y}}_d) \\ \mathbf{0} &= \hat{\boldsymbol{g}}(\hat{\boldsymbol{x}}, \hat{\boldsymbol{y}}, \hat{\boldsymbol{x}}_d) \ , \end{aligned} \qquad (12)$$

where $\hat{\boldsymbol{x}}_d$ and $\hat{\boldsymbol{y}}_d$ are the delayed state and algebraic variables, respectively.

In this study, the delays are included in the remote bus frequency measurements. The results in [12] show that time-synchronizing speed-based local and remote feedback signals has a destabilizing impact, regardless of the control method. Hence, we also consider non-time-synchronized signals. The delayed bus frequency signal $\omega_{\mathrm{B}id}$ is:

$$\omega_{\mathrm{B}id} = \omega_{\mathrm{B}i}(t - \tau(t)) \ , \qquad (13)$$

where $\tau(t)$ is the WAMS delay, which is of the form [13]:

$$\tau(t) = \tau_0 + \tau_p(t) + \tau_s(t) \ , \qquad (14)$$

where

- τ_0 is a constant component that expresses the processing time of the measurement unit plus the unavoidable latency imposed by the communication medium;

- $\tau_p(t)$ is a periodic component which implies that data packets are delivered in discrete time instants. It is $\tau_p(t) = t - t_k$, where t_k is the time when the last successfull data packet delivery occured; the delivery period of a packet without dropout is T;
- $\tau_s(t)$ is a stochastic component which accounts for uncertainties and noise. It is $\tau_s(t) = \frac{\mathrm{Gamma}(\alpha,\beta,\mathrm{t})}{1-p}$, which assumes a Gamma distribution with scale factor α, shape factor β [20]; p is the probability of a dropout.

The mean value of $\tau(t)$ is [13]:

$$\bar{\tau} = \tau_0 + \frac{T}{2(1-p)} + \frac{\alpha}{1-p}\beta \qquad (15)$$

The profile of WAMS delay model is illustrated in Fig. 3.
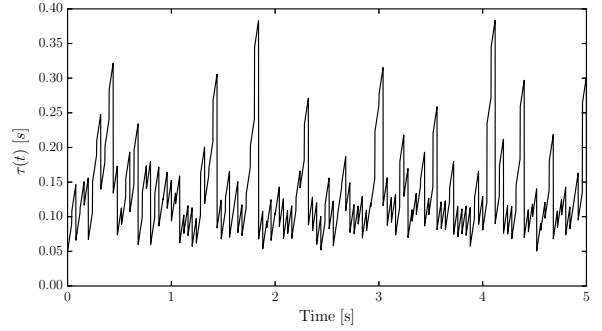

Fig. 3: WAMS delay ($\tau_0 = 0.05$ s, $T = 0.04$ s, $p = 0.2$, $\alpha = 0.02$, $\beta = 2$).

Modal observability/controllability analysis of DDAEs is not an easy task, since differentation of (12) leads to a transcendental characteristic equation, with infinitely many eigenvalues and associated eigenvectors [19]. Different techniques, e.g., Chebyshev discretization, Padé approximants [10], have been employed to overcome this problem. In this paper, we make use of the Padé approximants in order to approximate the effect of communication delays on wide-area signal observability.

B. Padé Approximants

Padé approximants are based on the well-known Taylor series expansion of $e^{-\tau s}$ in the frequency domain:

$$\begin{aligned} e^{-\tau s} &= 1 - \frac{\tau s}{1!} + \frac{(\tau s)^2}{2!} - \frac{(\tau s)^3}{3!} + ... \\ &\approx \frac{b_0 + b_1\tau s + ... + b_q(\tau s)^q}{a_0 + a_1\tau s + ... + a_p(\tau s)^p} \ , \end{aligned} \qquad (16)$$

where $a_0, a_1, ..., a_p$ and $b_0, b_1, ..., b_q$ are defined so that the first $p + q$ coefficients are the same as those of the Taylor expansion. The advantage of this approach is that it allows to represent a constant delay as a set of linear differential equations. Therefore, tracking the changes of the observabilities with respect to delays is relatively simple to implement through modal analysis. On the other hand, this technique is known to be of limited accuracy. Furthermore, it cannot

approximate properly crucial information of a WAMS delay, i.e., stochasticity and periodicity.

IV. CASE STUDY

The system considered in this study is shown in Fig. 4. It consists of two identical areas connected through a relatively weak tie; eleven buses $B1, B2, ..., B11$ and four synchronous machines $G1, G2, G3, G4$ connected at the medium voltage level of 20 kV; the nominal value of the high voltage transmission lines is 230 kV. Each machine is equipped with an AVR of type IEEE DC-1 and a turbine governor.

All results discussed in this section are obtained with Dome, a Python-based software tool for power system analysis [21].
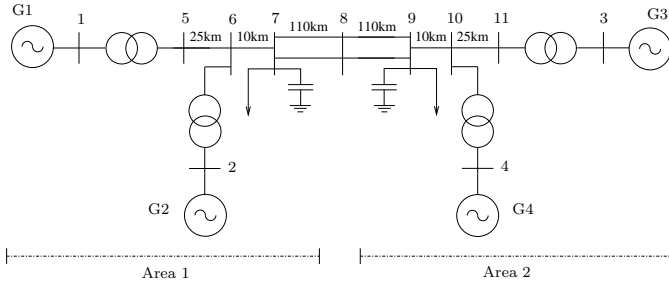

Fig. 4: Two-area four-machine test system.

A. Wide-Area Signals and Input Location Selection

Table I shows the critical modes of the two-area system. The most poorly damped mode is $\lambda_{1,2} = -0.095 \pm j3.5809$, which is an inter-area mode with the machines of Area 1 oscillating with respect to the ones of Area 2. The controllability of $\lambda_{1,2}$ from the four AVRs is presented in Table II.

TABLE I: Two-area system critical modes

Eigenvalue	Frequency (Hz)	Damping ratio (%)
$\lambda_{1,2} = -0.0958 \pm j3.5809$	0.57	2.67
$\lambda_{3,4} = -0.5144 \pm j6.8434$	1.09	7.50
$\lambda_{5,6} = -0.5993 \pm j6.6042$	1.06	9.04

TABLE II: Controllability of $\lambda_{1,2}$ from j-th AVR

j	1	2	3	4
gm_c	$2.12 \cdot 10^{-5}$	$2.04 \cdot 10^{-5}$	$3.10 \cdot 10^{-5}$	$3.01 \cdot 10^{-5}$

The geometric measures of $\lambda_{1,2}$ for local rotor speed signals are shown in Table III. If only local measurements are considered, the inter-area mode is better observable/controllable from G3.

TABLE III: Observability of $\lambda_{1,2}$ from ω_{Gj} and joint measure

Signal	gm_o	AVR	gm_c	gm_{co}
ω_{G3}	$2.22 \cdot 10^{-3}$	G3	$3.10 \cdot 10^{-5}$	$6.88 \cdot 10^{-8}$
ω_{G4}	$1.86 \cdot 10^{-3}$	G4	$3.01 \cdot 10^{-5}$	$5.61 \cdot 10^{-8}$
ω_{G1}	$2.01 \cdot 10^{-3}$	G1	$2.12 \cdot 10^{-5}$	$4.27 \cdot 10^{-8}$
ω_{G2}	$1.71 \cdot 10^{-3}$	G2	$1.71 \cdot 10^{-5}$	$3.48 \cdot 10^{-8}$

We consider wide-area signals as described in Section II. Two scenarios are examined: ideal bus frequencies (ω_{Bi}) estimated using the FDF; and bus frequencies obtained using SRF-PLL ($\tilde{\omega}_{Bi}$). Tables IV and V summarize the best signals and their geometric measures. The SRF-PLL has a negative impact on the observability of the mode by the wide-area signals.

The results for both scenarios suggest that differential frequencies $B5 - G3$ and $B1 - G3$ are the most suitable for damping the inter-area oscillation. Hence, in the remainder of the paper we assumed that the WAPSS is installed at G3. As expected, wide-area signals are more effective than local rotor speeds (Table III). Since B1 is the medium voltage side of the step-up transformer, it typically belongs to the generation side, and thus, a measurement at this point may not be available. For this reason, we proceed with the frequency $B5 - G3$.

TABLE IV: Candidates with best gm_{co} (ideal ω_{Bi}).

Signal	gm_o	AVR	gm_c	gm_{co}
$\omega_{B5} - \omega_{G3}$	0.00321	G3	$3.10 \cdot 10^{-5}$	$9.93 \cdot 10^{-8}$
$\omega_{B1} - \omega_{G3}$	0.00317	G3	$3.10 \cdot 10^{-5}$	$9.83 \cdot 10^{-8}$
$\omega_{B6} - \omega_{G3}$	0.00308	G3	$3.10 \cdot 10^{-5}$	$9.55 \cdot 10^{-8}$
$\omega_{B2} - \omega_{G3}$	0.00301	G3	$3.10 \cdot 10^{-5}$	$9.34 \cdot 10^{-8}$
$\omega_{B7} - \omega_{G3}$	0.00299	G3	$3.10 \cdot 10^{-5}$	$9.27 \cdot 10^{-8}$
$\omega_{B5} - \omega_{G4}$	0.00255	G4	$3.01 \cdot 10^{-5}$	$8.87 \cdot 10^{-8}$

TABLE V: Candidates with best gm_{co} ($\tilde{\omega}_{Bi}$ from SRF-PLL)

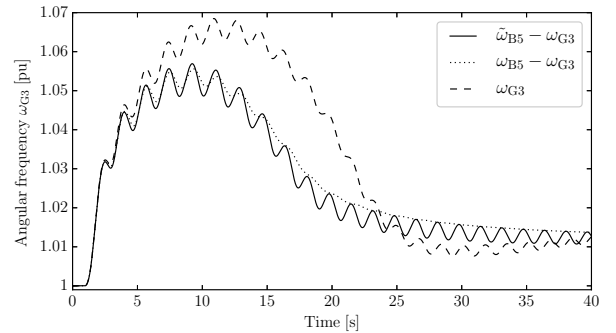| Signal	gm_o	AVR	gm_c	gm_{co}
$\tilde{\omega}_{B1} - \omega_{G3}$	0.00274	G3	$3.10 \cdot 10^{-5}$	$8.48 \cdot 10^{-8}$
$\tilde{\omega}_{B5} - \omega_{G3}$	0.00263	G3	$3.10 \cdot 10^{-5}$	$8.16 \cdot 10^{-8}$
$\tilde{\omega}_{B2} - \omega_{G3}$	0.00257	G3	$3.10 \cdot 10^{-5}$	$7.95 \cdot 10^{-8}$
$\tilde{\omega}_{B6} - \omega_{G3}$	0.00246	G3	$3.10 \cdot 10^{-5}$	$7.63 \cdot 10^{-8}$
$\tilde{\omega}_{B1} - \omega_{G4}$	0.00249	G4	$3.01 \cdot 10^{-5}$	$7.49 \cdot 10^{-8}$
$\tilde{\omega}_{B7} - \omega_{G3}$	0.00232	G3	$3.10 \cdot 10^{-5}$	$7.20 \cdot 10^{-8}$

Fig. 5: Rotor speed of G3 for local and wide-area control signals.

A time domain simulation is carried out with the WAPSS installed at G3 and imposing the outage of the load connected at B7 at $t = 1.0$ s. The implicit trapezoidal formula is used for the numerical integration of the system. The solution at

each time step is obtained by employing the Newton-Raphson iterative method.

Figure 5 shows the angular frequency of G3 for the local rotor speed ω_{G3} and the wide-area signals $\omega_{B5} - \omega_{G3}$ and $\tilde{\omega}_{B5} - \omega_{G3}$. The wide-area signal confirms to be the most effective to damp electromechanical oscillations. The observation that using the SRF-PLL to measure the bus frequency degrades the damping effect is also confirmed.

B. Effect of Time Delays

In this subsection, the impact of time delays on the damping effect of wide-area signals is examined. First, we attempt to approximate this effect using Padé polynomials. The joint observability/controllability of wide-area signals with respect to the time delay is shown in Fig. 6 and 7 for ideal and SRF-PLL estimated bus frequencies. The time delays degrade the observability of wide-area signals in both cases. In the region that is typical for network-induced delays, i.e., $50 - 150$ ms, the wide-area signals are still the best option to damping inter-area oscillations. For larger delays, however, i.e., $\tau > 400$ ms, results indicate that using the local rotor speed is more effective.
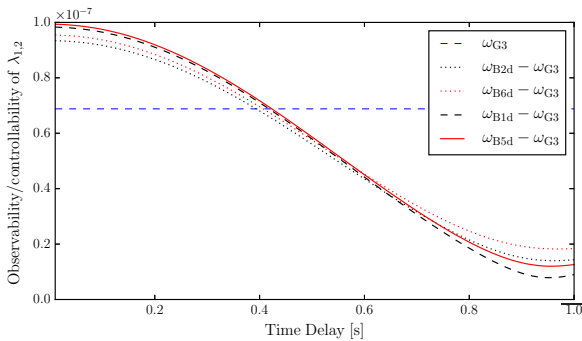

Fig. 6: Effect of approximated constant delays on the observability of wide-area signals (ideal ω_{Bi}).

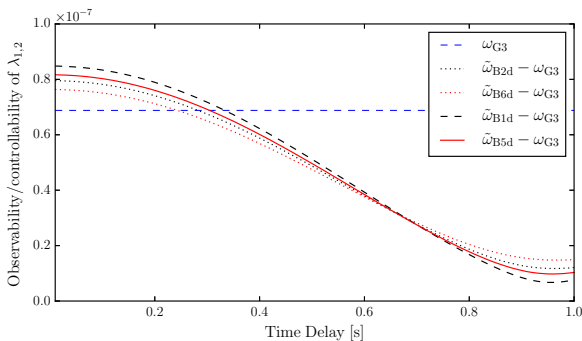

Fig. 7: Effect of approximated constant delays on the observability of wide-area signals ($\tilde{\omega}_{Bi}$ from SRF-PLL).

Since Padé polynomials provide an approximation of the delay effect, the results obtained in Figs. 6 and 7 are further

evaluated by carrying time domain simulation with inclusion of WAMS delays. Two delays, $\tau_1(t)$ and $\tau_2(t)$, with different expected (mean) values are examined. The parameters of the examined delays are given in Table VI. Both delays include a constant component of 50 ms, a periodic component with 40 ms delivery period and a 20% probability dropout rate. The two delays have different shape and scale factors of the Gamma distribution. Finally, the expected values are $\bar{\tau}_1 = 125$ ms and $\bar{\tau}_2 = 450$ ms, respectively.

TABLE VI: WAMS delays parameters

Delay $\tau_i(t)$	τ_0 [s]	T [s]	p	α	β	$\bar{\tau}_i$ [s]
$\tau_1(t)$	0.05	0.04	0.2	0.02	2.00	0.125
$\tau_2(t)$	0.05	0.04	0.2	0.10	3.00	0.450

Figures 8 and 9 show the angular frequency of G3 for ideal and SRF-PLL-based bus frequencies. The delays degrade the WAPSS damping ability. For the small delay ($\tau_1(t)$), the damping ability of the wide-area signal is better than using the local rotor speed. This is in agreement with the results obtained with Padé approximants. However, Figs. 8 and 9 suggest that the wide-area signal is clearly preferable even for large delays ($\tau_2(t)$), independently whether the ideal or SRF-PLL estimated bus frequency is used. This contradicts Padé approximant results.

Overall, we conclude that the study of a system using Padé approximants is reliable only if small delays are considered. Nevertheless, in order to assess whether the approximation for a considered delay is acceptable or not, i.e., whether a delay is small enough to trust Padé approximants, it is necessary to evaluate the results through detailed time domain simulations.
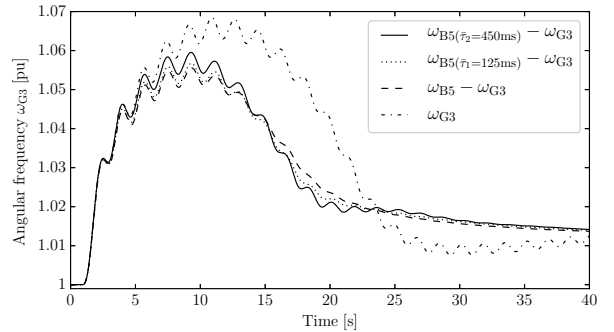

Fig. 8: Rotor speed of G3 (ideal ω_{Bi}).

V. Conclusions

The paper discusses a decentralized WAPSS with remote bus frequency measurements. Ideal bus frequency signals are compared with realistic measurement signals from PLLs that include measurement noise and delay. Modal and transient stability results based on the Kundur's two-area system show that wide-area signals are more effective that local signals to damp inter-area oscillations. Results also indicate that the PLL have a non-negligible and negative impact on the observability
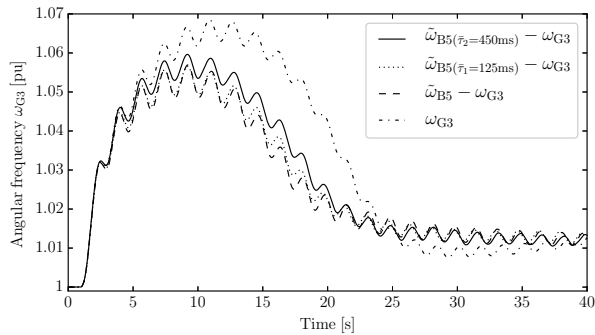
Fig. 9: Rotor speed of G3 ($\tilde{\omega}_{Bi}$ estimated with a SRF-PLL).

of the inter-area mode and, hence, on the overall damping ability of the WAPSS.

The impact of time delays on the observability of wide-area signals using Padé approximants is also investigated. Results show that this approach provides correct results only for "small" constant delays but it is not reliable for modal analysis of power systems with inclusion of WAMS delays. Further research will focus on exploiting eigen-based methods, such as [10], which allow carrying a global modal analysis of DDAEs.

REFERENCES

[1] P. Kundur, *Power system stability and control.* New York: Mc-Grall Hill, 1994.

[2] M. E. Aboul-Ela, A. A. Sallam, J. D. McCalley, and A. A. Fouad, "Damping controller design for power system oscillations using global signals," *IEEE Trans. on Power Systems*, vol. 11, no. 2, pp. 767–773, May 1996.

[3] J. H. Chow, J. J. Sanchez-Gasca, H. Ren, and S. Wang, "Power system damping controller design-using multiple input signals," *IEEE Control Systems Magazine*, vol. 20, no. 4, pp. 82–90, Aug. 2000.

[4] H. Wu, K. S. Tsakalis, and G. T. Heydt, "Evaluation of time delay effects to wide-area power system stabilizer design," *IEEE Trans. on Power Systems*, vol. 19, no. 4, pp. 1935–1941, Nov. 2004.

[5] A. Heniche and I. Kamwa, "Assessment of two methods to select wide-area signals for power system damping control," *IEEE Trans. on Power Systems*, vol. 23, no. 2, pp. 572–581, May 2008.

[11] C. Li, G. Li, C. Wang, and Z. Du, "Eigenvalue sensitivity and eigenvalue tracing of power systems with inclusion of time delays," *IEEE Trans. on Power Systems*, vol. 33, no. 4, pp. 3711–3719, July 2018.

[6] W. Yao, L. Jiang, Q. H. Wu, J. Y. Wen, and S. J. Cheng, "Delay-dependent stability analysis of the power system with a wide-area damping controller embedded," *IEEE Trans. on Power Systems*, vol. 26, no. 1, pp. 233–240, Feb. 2011.

[7] Y. Wang, P. Yemula, and A. Bose, "Decentralized communication and control systems for power system operation," *IEEE Trans. on Smart Grid*, vol. 6, no. 2, pp. 885–893, Mar. 2015.

[8] S. Wang, X. Meng, and T. Chen, "Wide-area control of power systems through delayed network communication," *IEEE Trans. on Control Systems Technology*, vol. 20, no. 2, pp. 495–503, Mar. 2012.

[9] B. P. Padhy, S. C. Srivastana, and N. Verma, "A wide-area damping controller considering network input and output delays and packet drop," *IEEE Trans. on Power Systems*, vol. 32, no. 1, pp. 166–176, Jan. 2017.

[10] F. Milano, "Small-signal stability analysis of large power systems with inclusion of multiple delays," *IEEE Trans. on Power Systems*, vol. 31, no. 4, pp. 3257–3266, July 2016.

[12] S. Ghosh, K. A. Folly, and A. Patel, "Synchronized versus non-synchronized feedback for speed-based wide-area PSS: Effect of time-delay," *IEEE Trans. on Smart Grid*, vol. 9, no. 5, pp. 3976–3985, Sep. 2018.

[13] M. Liu, I. Dassios, G. Tzounas, and F. Milano, "Stability analysis of power systems with inclusion of realistic-modeling of WAMS delays," *IEEE Trans. on Power Systems*, pp. 1–1, 2018.

[14] F. Milano and Á. Ortega, "Frequency divider," *IEEE Trans. on Power Systems*, vol. 32, no. 2, pp. 1493–1501, Mar. 2017.

[15] Á. Ortega and F. Milano, "Comparison of different PLL implementations for frequency estimation and control," in *Procs. of the 18th International Conference on Harmonics and Quality of Power (ICHQP)*, May 2018, pp. 1–6.

[16] H. Hamdan and A. Hamdan, "On the coupling measures between modes and state variables and subsynchronous resonance," *Electric Power Systems Research*, vol. 13, no. 3, pp. 165 – 171, 1987.

[17] Á. Ortega and F. Milano, "Comparison of bus frequency estimators for power system transient stability analysis," in *Procs. of the IEEE International Conference on Power System Technology (POWERCON)*, Sept 2016, pp. 1–6.

[18] ——, "Impact of frequency estimation for VSC-based devices with primary frequency control," in *Procs. of the IEEE PES Innovative Smart Grid Technologies Conference Europe (ISGT-Europe)*, Sept 2017, pp. 1–6.

[19] F. Milano and M. Anghel, "Impact of time delays on power system stability," *IEEE Trans. on Circuits and Systems - I: Regular Papers*, vol. 59, no. 4, pp. 889–900, Apr. 2012.

[20] O. Solomon and E. Fridman, "Systems with gamma-distributed delays: A lyapunov-based analysis," in *Procs. of the 52nd IEEE Conference on Decision and Control*, Dec 2013, pp. 318–323.

[21] F. Milano, "A Python-based software tool for power system analysis," in *Procs. of the IEEE PES General Meeting*, Vancouver, BC, Jul. 2013.